Versi Online: http://journal.ipb.ac.id/index.php/jtip
https://doi.org/10.6066/jtip.2026.37.1.44
Hasil Penelitian

Jurnal Teknologi dan Industri Pangan
Vol. 37(1): 44-54 Th. 2026 ISSN: 1979-7788
Terakreditasi Kemdiktisaintek: 295/C/C3/KPT/2026

Characterization of Acid-Treated Carbon from Snapper (*Lutjanidae*) and Red Grouper (*Epinephelus* spp.) Bones Using HCl and H_3PO_4

Mia Juliana*, Desak Ayu Sista Dewi

Industrial Engineering Study Program, Faculty of Engineering, Udayana University, Bali, Indonesia

Received December 5th 2024 / Revised October 25th 2025 / Accepted January 26th 2026

ABSTRACT

Fish processors usually discard fish bones as waste. The transformation of fish bones into carbon materials presents promising feasibility in view of sustainability. Acid-treated carbon is an inexpensive chemical adsorption material whose behavior is strongly related to its structural and compositional features. This work produced and characterized carbon materials from fish bone waste modified by H_3PO_4 and HCl. Snapper and red grouper (RG) fish bones were the raw materials. Heads of RG constituted 46.6% of the total weight, which is significantly higher than the 25.1% of snapper. While the bone and head of RG reached 18.11 and 17.38%, respectively, the snapper fish produced a higher percentage of 30% variability in nitrogen. The yield for acid treatment with H_3PO_4 was relatively higher (140%) than that of HCl (126.7%). The H_3PO_4-treated carbon showed FTIR peaks at 3646.58, 2989.79, 2348.43, and 1491.04 cm^{-1}, while the HCl-treated carbon produced peaks around 3630.19, 2340.72, 1318.4, 1058, and 659.68 cm^{-1}. The EDS analysis provided more carbon in HCl-treated samples (52.26%) than in H_3PO_4 (44.12%). The results provide initial compositional and structural analysis of acid-treated fish bone carbon. However, researchers should justify their practicability through additional experiments (e.g., BET surface area and adsorption performance tests) in the adsorption or water treatment fields.

Keywords: *carbon, EDS, fishbone, FTIR, SEM*

INTRODUCTION

A significant proportion of fish consumption creates waste, most notably non-edible parts that are usually discarded, like bones, fins, gills, scales, viscera, and skin (that is not further processed). An estimated 30–70% of each ton of fish processed becomes waste (Ahuja *et al.*, 2020). Similarly, Sahın, *et al.* (2018) reported that fish processing yields comprise 11.59% skin, 2.38% fins, 14.79% viscera, 57.92% carcass, and 14.49% head. According to these ratios, the estimated amount of annual waste generation is between 24.81 and 26.07 kg in the form of bone, 5.46 and 5.74 kg as viscera, and 7.46 and 7.83 kg as heads. These data suggest that the bones represent many fish by-products and are generally discarded without value-added use (Wulandari *et al.*, 2023).

Efforts to optimize fish waste management are therefore essential to reduce environmental burdens and create added value from by-products. One potential pathway is the conversion of fish bones into acid-treated carbon. Utilizing fish bones as raw material for acid-treated carbon aligns with sustainability principles by reducing waste, minimizing environmental impacts (Effendi *et al.*, 2018), and supporting the circular economy through resource valorization. This approach is particularly relevant in the fisheries industry, where the widely consumed and processed species such as snapper (*Lutjanidae*) and red grouper (*Epinephelus* spp.) generate large amounts of bones by product.

Acid activation is a fundamental modification technique, enabling structural and surface modification of the precursor through chemical interaction with acid solutions (Bhatti *et al.*, 2023). Although it does not always achieve the high porosity typical of fully activated carbon, it provides valuable insights into how chemical agents influence specific material properties (Budash *et al.*, 2023). In particular, it can enhance surface functional groups and modify elemental composition (Kolur *et al.*, 2019), which are key factors determining subsequent adsorption potential and suitability for further activation processes (Budash *et al.*, 2023).

Although numerous studies have explored carbon production from fish bone precursors using various activation techniques and species, few have systematically compared how different activating agents influence the resulting morphology and

*Corresponding Author: E-mail: mia.juliana@unud.ac.id

surface chemistry (Abdel-Ghani *et al.*, 2017; Lestari *et al.*, 2022; Ritonga *et al.*, 2022; Sihotang, 2019), most of these investigations have focused on individual activators or specific fish precursors in isolation. As a result, direct comparative analyses under similar conditions remain limited. Systematic evaluation of H_3PO_4 (Bhatti *et al.*, 2023; Neme *et al.*, 2022) and HCl (Setyaningrum *et al.*, 2024) treatments applied to bone-derived carbons, particularly from snapper (*Lutjanidae*) and red grouper (*Epinephelus* spp.), has not been extensively addressed. This comparative methodology is significant as selecting acid treatment and carbon yield, elemental composition, and functional group type are highly connected factors determining a precursor material's suitability for sustainable adsorbent application.

Therefore, this study aimed to produce acid-treated carbon from snapper (*Lutjanidae*) and red grouper (*Epinephelus* spp.) bones using H_3PO_4 and HCl as chemical agents, and to characterize the resulting materials through yield analysis, FTIR spectroscopy, and EDS composition. This approach provides essential baseline insights into the influence of acid treatment on fish bone-derived carbons, while contributing to the sustainable valorization of fishery by-products as potential precursors for advanced adsorbent materials for food processing aid applied in food industries.

MATERIALS AND METHOD

Materials

This study is an experimental research that utilizes fish bones as the main raw material for activated carbon production. Fish bone waste was collected from two commonly consumed species, namely snapper (*Lutjanidae*) and red grouper (*Epinephelus* spp.), obtained from Kedonganan Fish Market, Jimbaran, Bali, Indonesia. The activating agents used were phosphoric acid (H_3PO_4, 85%) and hydrochloric acid (HCl, 32%), both purchased from a local chemical supplier in Denpasar, Indonesia.

Methods

The experimental procedure was divided into two main stages. The first stage involved the preparation of raw material. Fish bones were manually separated from flesh, thoroughly washed with distilled water, and oven-dried (Oxone, 18 L, Indonesia) at 200 °C for 8 h until brittle. The dried bones were then ground using a laboratory blender to obtain finer particles.

The second stage was the chemical impregnation. Ten grams of bone powder were soaked separately in 15 mL of phosphoric acid (H_3PO_4, 85%) and hydrochloric acid (HCl, 32%) solutions. The mixtures were stirred and left to stand for 24 h at room temperature (29±1 °C, controlled under ambient laboratory conditions). Afterward, the impregnated samples were oven-dried at 200 °C for 8 h.

Subsequent analyses included measurement of bone morphology, carbon yield, and material characterization by Fourier Transform Infrared Spectroscopy (FTIR) and Energy Dispersive X-ray Spectroscopy (EDS). All experimental work was carried out at the Integrated Laboratory of Udayana University, Indonesia.

Physical characteristic of fish

Fish bone was characterized to determine the weight distribution of different body parts in two fish species, snapper (*Lutjanidae*) and red grouper (*Epinephelus* spp.). The body parts measured included head, tail, bones, viscera, and flesh, following the procedure described by Primawestri *et al.* (2023). Each part was carefully separated, weighed, and compared against the total body weight of the respective fish, as suggested by Tosin *et al.* (2021).

The same procedure was applied to both snapper and grouper samples to ensure consistency and comparability. The relative proportions of each body part (% of total weight) were calculated for both species, providing a baseline for evaluating the amount of bone available as precursor material. This comparative approach ensures that data from both fish groups are presented systematically, avoiding gaps in analysis and enabling a more precise assessment of species-specific variations.

Carbon and acid-treated carbon yield

The yield of acid-treated carbon was calculated to evaluate the efficiency of the production process and its potential implications for cost minimization. Yield determination was performed by weighing the dried carbon sample before and after acid treatment, following the procedure described by Lelawati (2015), and applying Equation 1.

$$\text{Carbon Yield (\%)} = \frac{\text{acid-treated carbon weight}}{\text{raw material weight}} \times 100 \quad (1)$$

Material molecular composition analysis by fourier transform infrared (FTIR)

This study employed FTIR analysis to identify functional groups in acid-treated carbons from bones using an IRPrestige-21 spectrophotometer (Shimadzu IRTracer-100, Shimadzu Corporation, Kyoto, Japan) at 4000–400 cm^{-1} with 4 cm^{-1} resolution. The results highlight chemical functionalities introduced by H_3PO_4 and HCl treatment, though comparison with the original fish bone spectra was not conducted and remains a direction for future research.

Material morphology and structure analysis by scanning electron microscopy (SEM)

Scanning Electron Microscopy (SEM) is a surface characterization technique that employs electron beams to achieve high-resolution imaging of solid materials. SEM analysis employed a JED-2300 Plus instrument with a DrySD™ detector (JEOL, Japan). Observations were conducted at magnifications up to 1000 times. SEM is beneficial for examining microstructural features such as surface morphology, pore distribution, and crack formation (Al Fath *et al.,* 2024). The technique provides topographical information that reveals surface protrusions, indentations, and porosity, thereby offering insights into the structural characteristics of the acid-treated carbons.

Identify the elemental composition of the material by energy dispersive spectroscopy (EDS)

Energy Dispersive Spectroscopy (EDS) was employed to determine the elemental composition of the samples. The analysis used a JED-2300 Plus system with a DrySD™ (Dry Silicon Drift Detector) (JEOL, Japan), fully integrated with SEM. EDS enables the detection of both major elements and trace contaminants within the material, thereby complementing the morphological data obtained from SEM. This combined approach is widely applied to characterize carbon-based materials elemental distribution and chemical composition (Ratnasari *et al.*, 2024).

RESULTS AND DISCUSSION

The physical characteristic of fish

This study selected large-sized fish to obtain more bone weight, specifically grouper (*Epinephelus* spp.) and snapper (*Lutjanidae*), as shown in Figures 1. The results indicate that grouper exhibited a heavier head weight of 46.6% compared to its flesh, which accounted for only 19.8%. This finding is consistent with (Prakoso, 2019; Purnomo, 2020), who reported that grouper skull bones are characterized by strong and solid structures and a flattened body shape, leading to a lighter flesh weight relative to the head. In contrast, snapper presented a higher proportion of flesh weight at 53.2%, compared to its head weight of only 25.1% (Figure 1). According to Purnomo (2020), the edible portion of snapper flesh (red meat) generally constitutes around 50% of the total body weight.

Carbon yield

In this study, only the bones and heads were utilized as carbon precursors, while other body parts, such as flesh, tails, and viscera, were excluded due to their lower solid fraction. After the dewatering stage (Figure 2), the resulting material appeared black to dark brown, with a hard and porous texture. The dark coloration suggests partial carbonization occurred, where a substantial portion of the organic matrix decomposed into carbon, while the brownish tint indicates incomplete transformation.

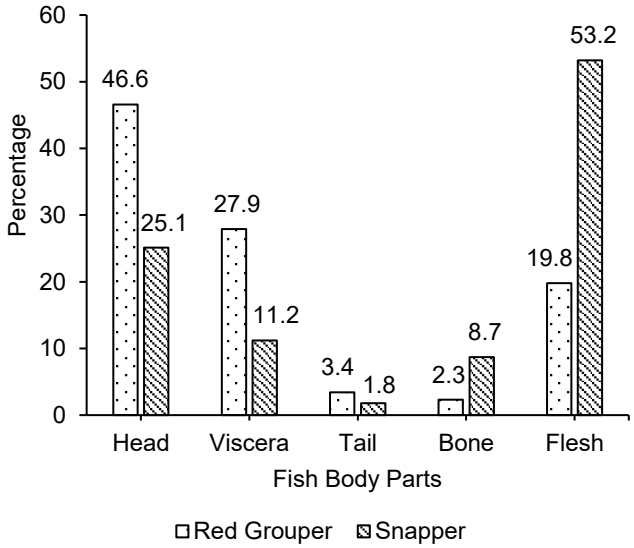

Figure 1. Body part weight relative of grouper and snapper

Figure 2. The fish bones and heads that have been dried until become carbonised

However, it is important to note that the heating treatment applied 200 °C for 8 h in a conventional oven following acid soaking does not represent complete carbonization under standard definitions. Typically, carbonization is performed at 400–800 °C under an inert atmosphere (e.g., nitrogen or argon) to ensure complete thermal decomposition and development of porous carbon structures. This study obtained acid-treated carbon rather than fully activated carbon.

The drying process led to weight reduction from initial wet samples of 276 g (red grouper, *Epinephelus*

spp.) and 374 g (snapper, *Lutjanidae*) to yields of 18.11% and 17.38%, respectively. Lower moisture content and higher bone density likely produced the slightly higher yield of grouper bone carbon, aligning with reports that grouper bones are structurally denser than snapper bones (Prakoso, 2019; Purnomo, 2020).

Drying yields depend on several interrelated factors, including drying temperature, ambient humidity, material thickness, initial moisture content, and the drying equipment employed. Higher temperatures can accelerate water removal by increasing evaporation rates (Santi *et al.*, 2021). Low ambient humidity enhances drying efficiency by promoting moisture transfer to the surrounding air (Rahayuningtyas and Kuala, 2016). The physical characteristics of the sample also play an important role; thicker materials generally require longer drying times than thinner ones, and samples with higher initial moisture content undergo more prolonged dehydration (Hasibuan and Ridhatullah, 2019). Furthermore, the choice of drying method and equipment significantly affects the overall efficiency and quality of the drying outcome (Hasibuan and Ridhatullah, 2019).

Acid-treated carbon yield

In this study, the carbon obtained from fish bones was subjected to acid treatment, commonly called chemical activation. The soaking process with acids aims to degrade residual organic molecules or impurities formed during carbonization (Putrianda *et al.*, 2019), enhance pore opening to potentially increase surface reactivity, and improve the material's effectiveness in subsequent applications (Kwak *et al.*, 2022; Tani and Lumingkewas, 2022). The yield of acid-treated carbon was determined by comparing the dry weight of the raw carbon sample with the dry weight after acid soaking and drying (Abdel-Ghani *et al.*, 2017).

The treatment with H_3PO_4 solution produced a yield of 140% (dry weight 21 g), higher than the HCl treatment, which yielded 126.7% (after drying weight 19 g). Neme *et al.* (2022) found that phosphoric acid treatment often yields higher yields. A high impregnation ratio of approximately 4.39:1 (50 mL of 85% H_3PO_4 and HCl per 15 g of carbon) was applied, which likely caused chemical retention within the carbon matrix, thereby increasing its mass. (Heidarinejad *et al.*, 2020) also noted that phosphoric acid at relatively low treatment temperatures produces higher yields and larger surface areas. Liu *et al.* (2022) added that using H_3PO_4, which requires a lower temperature, can shorten the activation time and improve the activation efficiency. The drying process also affects the yield produced. The study used a temperature of 200 °C for 8 h. Research by Adebisi *et al.* (2016) states that the correct temperature and drying duration will influence the yield obtained. Yield decreases when there is an increase in temperature, concentration, and time.

In this study, using high impregnation ratio of approximately 4.39:1 may led to over activation. Yakout and El-Deen (2016) stated that over-activation can occur under excessive impregnation, leading to partial degradation of the carbon framework, and excessive formation of functional groups, pore blockage, and reduced effective porosity. Timur *et al.* (2006) added that excess phosphoric acid may promote char gasification and increase total weight loss. Therefore, while the high yield in this study reflects chemical incorporation from acid treatment, further characterization, such as porosity and surface area analysis, would be required to confirm its potential as functional activated carbon.

Material molecular composition analysis by fourier transform infrared spectroscopy (FTIR)

Earlier studies have identified natural organic and inorganic functional groups in raw fish bones. For instance, the FTIR spectra of the raw fish bones usually present protein associated peaks at amide I (1649–1662 cm^{-1}), amide II (1548–1552 cm^{-1}), and amide III (1242–1244 cm^{-1}) in addition to phosphate bands located between 565 and 569 cm^{-1} as well as at 605 cm^{-1} assigned to hydroxyapatite (Fatmawati *et al.*, 2025). These characteristics are evidence of collagen–phosphate composition in the raw fish bones before activation.

Remarkable changes were found in this study for fish bone-based carbon after the acid treatment. The FTIR spectrum of H_3PO_4 modified carbon shows a broad band around 3400 cm^{-1} corresponding to O–H stretching vibrations, indicating that the activation process introduced hydroxyl groups, which enhance both the adsorption capacity and the hydrophilic nature of the material (Ana *et al.*, 2022; Hernández-Barreto *et al.*, 2022). Additional peaks appeared around 1700 cm^{-1} correspond to C=O, C=C, and C=N vibrations, all of them associated to collagen and other proteins (Hernández-Barreto *et al.*, 2022) and 1600–1500 cm^{-1} (aromatic C=C), indicating structural transformation of the carbon matrix and incorporation of oxygenated functional groups (Mohammed *et al.*, 2022). Peaks in the 1000–1200 cm^{-1} region were associated with C–O stretching from alcohols, ethers, or phenols, consistent with forming new surface functionalities during phosphoric acid treatment (Smith, 2024; Vasdazara *et al.*, 2018).

According to Ana *et al.* (2022), for the activated carbon, a strong absorption band is generally observed in the vicinity of 3400 cm^{-1}, possibly due to the hydroxyl group's O–H stretching vibration. These hydroxyl functions are crucial to the adsorption of polar molecules, especially as the active sites for hydrogen bonding and surface interactions. The spectrum of H_3PO_4 activated carbon also showed a

shallow band located at around 2900 cm^{-1}, corresponding to the C–H stretching vibrations of residual organic alcoholic impurities (Abdel-Ghani *et al.*, 2017).

By contrast, the FTIR spectrum of HCl acid-treated carbon exhibited a distinct absorption band at 3630 cm^{-1} corresponding to O–H stretching vibrations (Ana *et al.*, 2022; Hart *et al.*, 2023), but with noticeably lower intensity than that of H_3PO_4 activated carbon. A peak at 2340 cm^{-1} was associated with adsorbed CO_2 (Mihaylov *et al.*, 2016), likely originating from atmospheric contamination during sample preparation. Additional peaks at 1318 and 1058 cm^{-1} correspond to O–H or C–O bending vibrations, indicating the presence of reflects hydrogen bond in H_2O/-OH/NH_3/-NH_2 (Nandiyanto *et al.*, 2019), while the band at 659 cm^{-1} reflects aromatic ring deformation or crystal lattice vibrations (Nandiyanto *et al.*, 2019).

This observation suggests the carbonisation process was not completely exhaustive, leaving minor organic fragments derived from fish bone precursors. Furthermore, the strong band detected around 1700 cm^{-1} confirms the presence of carbonyl groups, possibly from carboxylic acids, esters, or ketones (Hernández-Barreto *et al.*, 2022; Mohammed *et al.*, 2022). These oxygenated groups enhance adsorption capacity through dipole–dipole interactions and electron donor–acceptor mechanisms. The peaks at 1600–1500 cm^{-1} represent aromatic C=C stretching, indicating the formation of a stable aromatic network structure (Mohammed *et al.*, 2022; Nandiyanto *et al.*, 2019). Aromatic domains provide rigidity and contribute to the high surface stability of the carbon. Additional peaks in the region of 1000–1200 cm^{-1} were associated with C–O stretching vibrations of ethers, alcohols, or phenolic groups (Smith, 2024; Vasdazara *et al.*, 2018), further supporting the presence of oxygenated surface functionalities. The sharpness and distinctness of these peaks indicate a relatively pure and well-developed carbon structure, with minimal spectral overlap suggesting low contamination levels.

Material morphology and structure analysis by scanning electron microscopy (SEM)

SEM analysis revealed apparent differences in pore morphology between carbons activated with HCl and H_3PO_4. Activation using HCl produced a heterogeneous porous structure (Figure 3A), characterized by small and large pores that appeared more numerous and widely distributed across the carbon matrix. The presence of meso–macropores suggests that HCl primarily acts through demineralization and etching mechanisms, which remove inorganic components and enlarge existing voids, thereby creating hierarchical porosity. This finding is consistent with previous research by Tan *et al.* (2017) and Verayana *et al.* (2018), which demonstrated that HCl activation produces carbon with higher porosity and larger surface area.

In contrast, H_3PO_4 activation generated a more uniform surface morphology dominated by smaller pores, indicating a predominance of microporous structures (shown in Figure 3B). The result aligns with research conducted by Heidarinejad *et al.* (2020) and Sirimuangjinda *et al.* (2012), who found that H_3PO_4 activation produces carbon with microporous structures. This pattern implies that phosphoric acid promotes pore development mainly through chemical crosslinking and stabilization of the carbon skeleton, which restricts excessive pore widening but enhances micropore formation (Tan *et al.*, 2017).

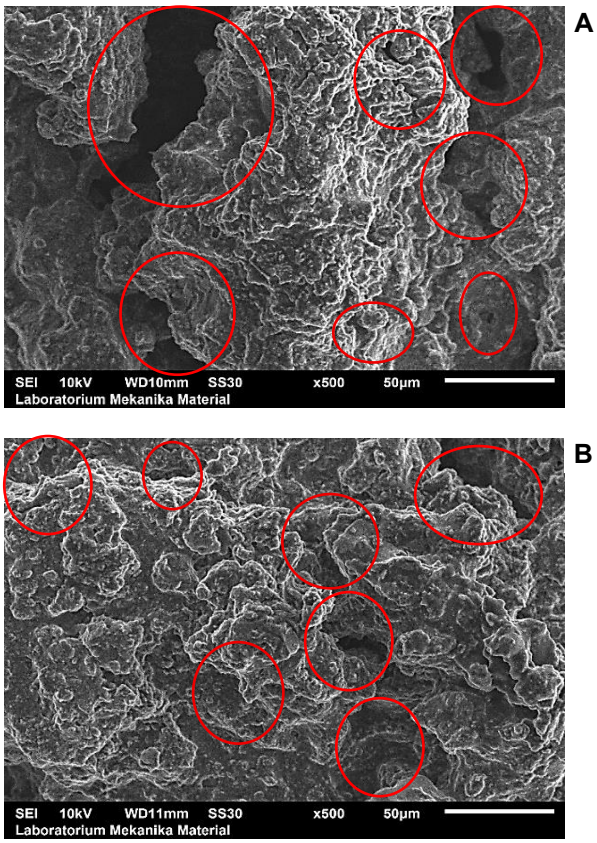

Note: HCl activator (A); H_3PO_4 activator (B)

Figure 3. Pore appearance of (A) HCl activated carbon 500x magnification and of (B) H_3PO_4 activated carbon with 500x magnification

FTIR spectra strongly support these morphological differences. As shown in Figure 4A, H_3PO_4 activation produced distinct peaks at ~3400 cm^{-1} (O–H stretching), 1700 cm^{-1} (C=O stretching), 1600–1500 cm^{-1} (aromatic C=C), and 1000–1200 cm^{-1} (C–O and P–O–C stretching) (Ana *et al.*, 2022; Hernández-Barreto *et al.*, 2022). These bands

confirm the effect of acid treatment on incorporating oxygenated and phosphate-related functional groups, stabilizing the aromatic framework, and promoting micropore development. On the other hand, shown in Figure 4B, HCl activated carbon exhibited peaks at 3630 cm^{-1} (isolated O–H), 2340 cm^{-1} (adsorbed CO_2), 1318–1058 cm^{-1} (C–O stretching), and 659 cm^{-1} (aromatic ring deformation or lattice vibration) (Mihaylov *et al.*, 2016; Mohammed *et al.*, 2022; Nandiyanto *et al.*, 2019). The dominance of such bands indicates strong mineral removal and structural rearrangement, consistent with the forma-tion of larger meso–macropores observed in SEM images.

Research by Fito *et al.* (2023) report that the adsorbent material possesses high porosity and a heterogeneous surface morphology, characterized by numerous surface fissures and irregularities. These features indicate an expanded specific surface area, which enhances the material's potential for adsorption applications. The observed structural complexity supports its suitability for capturing various contaminants through physical or chemical interactions.

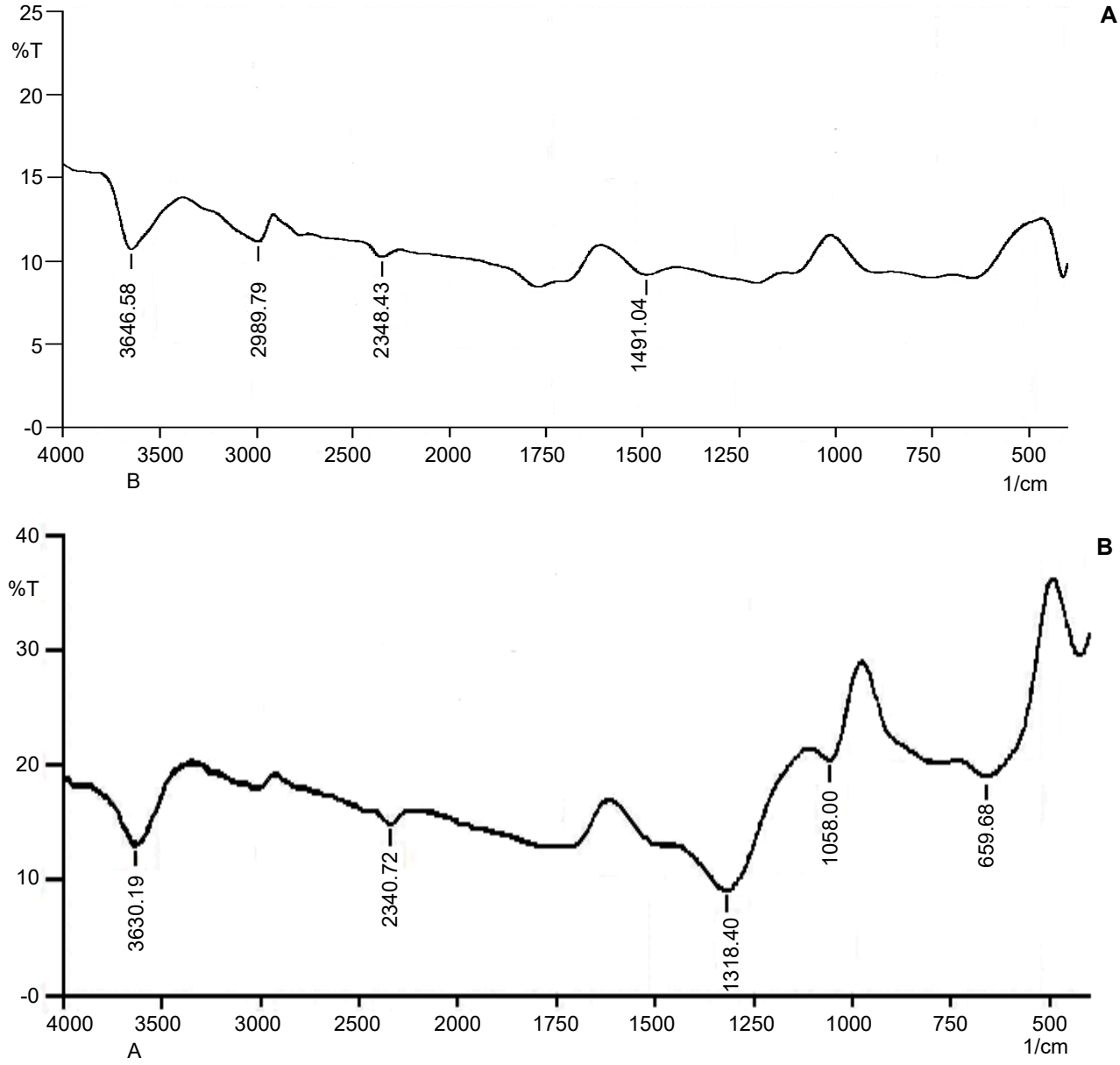

Note: H_3PO_4 activator (A); HCl activator (B)

Figure 4. FTIR spectra of acid-treated carbon derived from the combined fish bone waste of *Lutjanus sp.* (snapper) and *Epinephelus sp.* (red grouper), activated using (A) H_3PO_4 and (B) HCl, recorded within the wavenumber range of 4000–400 cm^{-1}

Nevertheless, this study is limited by the absence of complementary characterizations such as BET (Fito *et al.,* 2023) surface area and pore size distribution analysis, which are crucial to quantitatively validate the observed porosity. Additionally, surface chemical composition could be more precisely analyzed using techniques like XPS or Boehm titration, while Raman spectroscopy (Sirimuangjinda *et al.*, 2012) would provide insight into the degree of structural disorder caused by potential over-activation at high impregnation ratios. Addressing these limitations in future research would allow a more comprehensive understanding of the relationship between activation chemistry, surface functionality, and morphological development that future work will include FTIR characterization of the raw fish bone to provide a more comprehensive comparison and confirm the chemical transformation induced by acid treatment. FTIR characterization of the raw fish bone will provide a more extensive comparison and confirm the chemical transformation induced by acid treatment needed in future work.

Identity the elemental composition of the material by energy dispersive X-ray spectroscopy (EDS)

To strengthen the SEM findings, additional characterization was conducted using EDS (Energy Dispersive X-ray Spectroscopy) to verify the elemental composition and assess the removal of residual contaminants (Al-sareji *et al.,* 2024; Ratnasari *et al.,* 2024). Based on the EDS spectrum of HCl-activated carbon (Figure 5A), the material exhibited a dominant carbon content of 52.26%, confirming carbon as the primary constituent of activated carbon. Oxygen was also detected at 22.99%, indicating the incorporation of oxygenated groups during chemical activation. In addition, relatively high chlorine (Cl) content of 10.10% was observed, along with aluminium (Al) 0.62%, phosphorus (P) 4.62%, and calcium (Ca) 9.41%. The presence of these elements may arise from processing conditions and material handling during activation. These results suggest that HCl activation not only enriches the carbon matrix, but also introduces oxygen-containing functionalities that may enhance adsorption capacity. However, this section requires a reference or comparison with the original composition of fish bone powder, as no supporting reference is currently provided.

Similarly, the EDS spectrum of H_3PO_4 activated carbon (Figure 5B) revealed a carbon content of 44.12% and oxygen at 19.11%, consistent with the formation of oxygenated groups during activation. The spectrum also showed chlorine (Cl) at 10.10%, calcium (Ca) at 9.21%, phosphorus (P) at 5.05%, and sodium (Na) at 0.47%. Notably, the chlorine and calcium concentrations are relatively high rather than negligible, indicating incomplete removal of residual inorganic species during the activation process. These findings confirm that H_3PO_4 activation produces carbon materials enriched with oxygen functionalities, although residual elemental contaminants may still persist.

CONCLUSION

Acid-treated carbons can be prepared from fish bone waste using carbonization and chemical activation. Carbonizing the organic part of fish bone leads to a high content of inorganic residue. It produces a carbon-enriched matrix with surface modification and the possibility of pore formation upon further chemical activation (HCl or H_3PO_4). The chemical functional groups and surface morphology of the as-obtained carbon samples were characterized using FTIR and SEM analyses. The present results demonstrate that the acid-treated carbon derived from fish bones exhibits distinct surface morphological features and pore structures, which may be beneficial for potential adsorption or material applications. Therefore, the carbon materials derived from fish bone waste show potential as low-cost adsorbents for impurity removal in food processing, although further studies are required to evaluate their adsorption performance, including BET surface area and porosity measurements, should be proposed to validate activation depth and adsorption capacities.

ACKNOWLEDGEMENT

The researcher would like to thank to LPPM Udayana University for the contribution in funding the research to completion.

REFERENCES

Abdel-Ghani, N. T., El-Chaghaby, G. A., Rawash, E.-S. A., & Lima, E. C. (2017). Adsorption of coomassie brilliant blue R-250 dye onto novel activated carbon prepared from *Nigella sativa* L. waste: Equilibrium, kinetics and thermodynamics running title: Adsorption of brilliant blue dye onto *Nigella sativa* L. waste activated carbon. *Journal of the Chilean Chemical Society*, *62*(2), 3505–3511. https://doi.org/10.4067/S0717-97072017000200016

Adebisi, G. A., Chowdhury, Z. Z., Abd Hamid, S. B., & Ali, E. (2016). Hydrothermally treated banana empty fruit bunch fiber activated carbon for Pb(II) and Zn(II) removal. *BioResources*, *11*(4), 9686–9709. https://doi.org/10.15376/biores.11.4.9686-9709

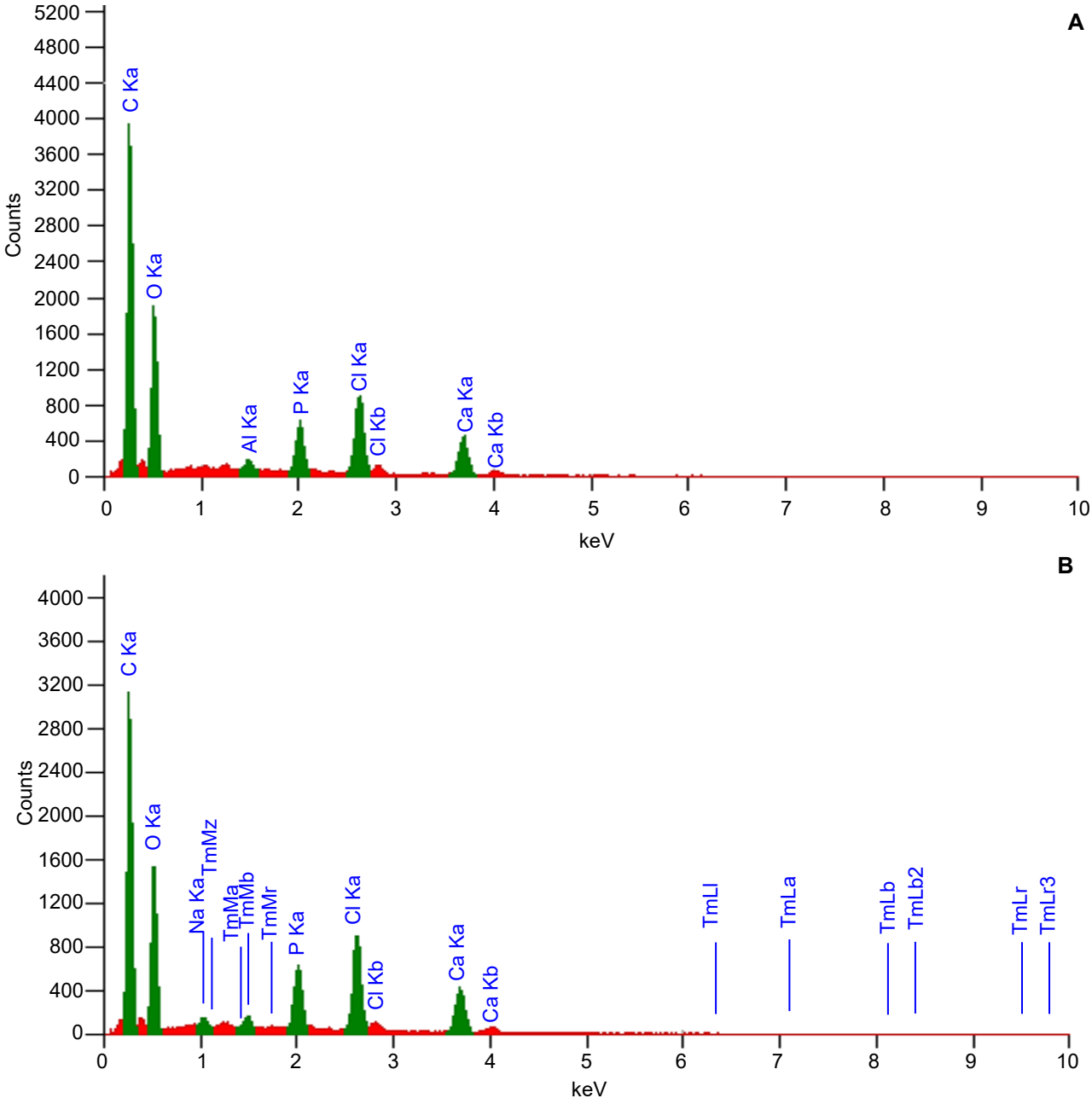

Note: HCl activator (A); H_3PO_4 activator (B)

Figure 5. Energy-dispersive X-ray spectroscopy (EDS) spectra showing the elemental composition of acid-treated carbon (A) HCl and (B) H_3PO_4. K-alpha (Ka) and K-beta (Kb) are K electron shell

Ahuja, I., Dauksas, E., Remme, J. F., Richardsen, R., & Løes, A.-K. (2020). Fish and fish waste-based fertilizers in organic farming – With status in Norway: A review. *Waste Management*, *115*, 95–112. https://doi.org/10.1016/j.wasman.2020.07.025

Al Fath, M. T., Sarah, M., Hasibuan, G. C. R., Alifia, K., Siagian, A., & Natasya, T. (2024). Physical properties of pectin edible film with kepok banana blossom filler as food packaging. *IOP Conference Series: Earth and Environmental Science*, *1352*, 012007. https://doi.org/10.1088/1755-1315/1352/1/012007

Al-sareji, O. J., Grmasha, R. A., Meiczinger, M., Al-Juboori, R. A., Somogyi, V., & Hashim, K. S. (2024). A sustainable banana peel activated carbon for removing pharmaceutical pollutants from different waters: Production, characterization, and application. *Materials*,

17(5), 1032. https://doi.org/10.3390/ma17051032

Ana, I. D., Lestari, A., Lagarrigue, P., Soulie, J., Anggraeni, R., Maube-Bosc, F., Thouron, C., Duployer, B., Tenailleau, C., & Drouet, C. (2022). Safe-by-design antibacterial peroxide-substituted biomimetic apatites: Proof of concept in tropical dentistry. *Journal of Functional Biomaterials*, *13*(3), 144. https://doi.org/10.3390/jfb13030144

Bhatti, A. H., Waris, M., Kazmi, W. W., Kang, K.-H., & Bhatti, U. H. (2023). Acid-treated activated carbon as simple and inexpensive catalyst to accelerate CO_2 desorption from aqueous amine solution. *Carbon Capture Science & Technology*, *8*, 100131. https://doi.org/10.1016/j.ccst.2023.100131

Budash, Y., Plavan, V., Tarasenko, N., Ishchenko, O., & Koliada, M. (2023). Effect of acid modification on porous structure and adsorption properties of different type Ukrainian clays for water purification technologies. *Journal of Ecological Engineering*, *24*(5), 210–221. https://doi.org/10.12911/22998993/161691

Effendi, R., Salsabila, H., & Malik, A. (2018). Pemahaman tentang lingkungan berkelanjutan. *MODUL*, *18*(2), 75–82. https://doi.org/10.14710/mdl.18.2.2018.75-82

Fatmawati, S., Istiqomah, S. M., Hasanah, N., Helan, M. E. I. K., Santoso, M., Nugraheni, Z. V., Jadid, N., Adi, A. C., & Rachmawati, H. (2025). Physico-chemical characterization of natural nano calcium extracted from different fish bones in catfish (*Clarias gariepinus*) and snakehead fish (*Channa striata*). *Case Studies in Chemical and Environmental Engineering*, *11*, 101080. https://doi.org/10.1016/j.cscee.2024.101080

Fito, J., Abewaa, M., Mengistu, A., Angassa, K., Ambaye, A. D., Moyo, W., & Nkambule, T. (2023). Adsorption of methylene blue from textile industrial wastewater using activated carbon developed from *Rumex abyssinicus* plant. *Scientific Reports*, *13*, 5427. https://doi.org/10.1038/s41598-023-32341-w

Hart, A., Porbeni, D. W., Omonmhenle, S., & Peretomode, E. (2023). Waste bone char-derived adsorbents: Characteristics, adsorption mechanism and model approach. *Environmental Technology Reviews*, *12*(1), 175–204. https://doi.org/10.1080/21622515.2023.2197128

Hasibuan, R., & Ridhatullah, M. A. (2019). Pengaruh ketebalan bahan dan jumlah desikan terhadap laju pengeringan jahe (*Zingiber officinale* Roscoe) pada pengering kombinasi surya dan desikan. *Jurnal Teknik Kimia USU*, *8*(2), 61–66. https://doi.org/10.32734/jtk.v8i2.1882

Heidarinejad, Z., Dehghani, M. H., Heidari, M., Javedan, G., Ali, I., & Sillanpää, M. (2020). Methods for preparation and activation of activated carbon: A review. *Environmental Chemistry Letters*, *18*, 393–415. https://doi.org/10.1007/s10311-019-00955-0

Hernández-Barreto, D. F., Hernández-Cocoletzi, H., & Moreno-Piraján, J. C. (2022). Biogenic hydroxyapatite obtained from bone wastes using CO_2-assisted pyrolysis and its interaction with glyphosate: A computational and experimental study. *ACS Omega*, *7*(27), 23265–23275. https://doi.org/10.1021/acsomega.2c01379

Kolur, N. A., Sharifian, S., & Kaghazchi, T. (2019). Investigation of sulfuric acid-treated activated carbon properties. *Turkish Journal of Chemistry*, *43*(2), 663–675. https://doi.org/10.3906/kim-1810-63

Kwak, C. H., Lim, C., Kim, S., & Lee, Y.-S. (2022). Surface modification of carbon materials and its application as adsorbents. *Journal of Industrial and Engineering Chemistry*, *116*, 21–31. https://doi.org/10.1016/j.jiec.2022.08.043

Lelawati. (2015). Optimalisasi suhu karbonisasi terhadap rendemen pada proses pembuatan arang aktif. *Majalah Teknis Simes*, *9*(2), 1–5.

Lestari, S., Nurhadi, M., Wardani, R. K., Saputro, E., Pujisupiati, R., Muskita, N. S., Fortuna, N., Purwandari, A. S., Aryani, F., Lai, S. Y., & Nur, H. (2022). Comparative adsorption performance of carbon-containing hydroxyapatite derived Tenggiri (*Scomberomorini*) and Belida (*Chitala*) fish bone for methylene blue. *Bulletin of Chemical Reaction Engineering & Catalysis*, *17*(3), 565–576. https://doi.org/10.9767/bcrec.17.3.15303.565-576

Liu, J., Zhang, K., Wang, H., Lin, L., Zhang, J., Li, P., Zhang, Q., Shi, J., & Cui, H. (2022). Advances in micro-/mesopore regulation methods for plant-derived carbon materials. *Polymers*, *14*(20), 4261. https://doi.org/10.3390/polym14204261

Mihaylov, M., Chakarova, K., Andonova, S., Drenchev, N., Ivanova, E., Sabetghadam, A., Seoane, B., Gascon, J., Kapteijn, F., & Hadjiivanov, K. (2016). Adsorption forms of CO_2 on MIL-53(Al) and NH_2-MIL-53(Al) as revealed by FTIR Spectroscopy. *The Journal of Physical Chemistry C*, *120*(41), 23584–23595. https://doi.org/10.1021/acs.jpcc.6b07492

Mohammed, H. Y., Farea, M. A., Sayyad, P. W., Ingle, N. N., Al-Gahouari, T., Mahadik, M. M., Bodkhe, G. A., Shirsat, S. M., & Shirsat, M. D. (2022). Selective and sensitive chemiresistive sensors based on polyaniline/graphene oxide nanocomposite: A cost-effective approach. *Journal of Science: Advanced Materials and Devices*, *7*(1), 100391. https://doi.org/10.1016/j.jsamd.2021.08.004

Nandiyanto, A. B. D., Oktiani, R., & Ragadhita, R. (2019). How to read and interpret FTIR spectroscope of organic material. *Indonesian Journal of Science and Technology*, *4*(1), 97–118. https://doi.org/10.17509/ijost.v4i1.15806

Neme, I., Gonfa, G., & Masi, C. (2022). Activated carbon from biomass precursors using phosphoric acid: A review. *Heliyon*, *8*(12), e11940. https://doi.org/10.1016/j.heliyon.2022.e11940

Prakoso, A. A. (2019). *Ikan Kerapu – Taksonomi, Ciri, Morfologi, Habitat, Jenis & Karakteristik*. https://rimbakita.com/kerapu/

Primawestri, M., Sumardianto, & Kurniasih, R. A. (2023). Karakteristik stik ikan lele (*Clarias gariepinus*) dengan perbedaan rasio daging dan tulang. *Jurnal Ilmu dan Teknologi Perikanan*, *5*(1), 44–51.

Purnomo, G. (2020). *Melek Perikanan*. https://www.melekperikanan.com/2020/02/habitat-morfologi-dan-klasifikasi-ikan_24.html

Putrianda, D. C., Yuliana, L., & Budiastuti, H. (2019). Aktivasi karbon aktif kulit singkong dengan aktivator NaCl, $ZnCl_2$, dan Na_2CO_3 untuk adsorben Pb^{2+}. *Prosiding Seminar Nasional Terapan Riset Inovatif*, *5*, 274–281.

Rahayuningtyas, A., & Kuala, S. I. (2016). Pengaruh suhu dan kelembaban udara pada proses pengeringan singkong (Studi kasus: Pengering tipe rak). *Ethos: Jurnal Penelitian dan Pengabdian*, *4*(1), 99–104. https://doi.org/10.29313/ethos.v0i0.1663

Ratnasari, R., Wardhani, G. A. P. K., & Taufiq, A. (2024). Bio-oil quality based on coconut carbon biomass using pyrolisis method. *Indonesian Journal of Chemical Research*, *12*(2), 153–163. https://doi.org/10.30598/ijcr.2024.12-rif

Ritonga, F. S., Humaidi, S., & Sitorus, Z. (2022). Synthesis of carbon from yellowfin tuna fishbone to remove iron (Fe) metal in well water from Bandar Setia. *Journal of Physics: Conference Series*, *2376*, 012001. https://doi.org/10.1088/1742-6596/2376/1/012001

Sahın, A. G., Tepe, R., & İspir, Ü. (2018). The investigation of meat yield of *Acanthobrama marmid* Heckel, 1843 from Karakaya Dam Lake. *Süleyman Demirel Üniversitesi Fen Bilimleri Enstitüsü Dergisi*, *22*(Special), 536–540. https://doi.org/ 10.19113/sdufbed.83580

Santi, N. I., Utama, I. M. S., & Madrini, I. A. G. B. (2021). Pengaruh suhu dan waktu pengeringan terhadap karakteristik fisikokimia buah naga merah (*Hylocereus polyrhizus* (Weber) Britton & Rose) kering. *Jurnal Hortikultura Indonesia*, *12*(1), 69–80. https://doi.org/10.29244/jhi.12.1.69-80

Setyaningrum, D., Fajarwati, N., & Maghfiroh, A. M. (2024). The effect of HCL activator concentration on the effectiveness of activated carbon derived from corncobs for methylene blue adsorption. *SPIN Jurnal Kimia & Pendidikan Kimia*, *6*(2), 181–193. https://doi.org/10.20414/spin.v6i2.11516

Sihotang, M. S. (2019). Model program processing of fishbone waste transfer for the application of drinking water products and test characterization. *Journal of Technomaterial Physics*, *1*(1), 39–46. https://doi.org/10.32734/jotp.v1i1.827

Sirimuangjinda, A., Atong, D., & Pechyen, C. (2012). Comparison on pore development of activated carbon produced from scrap tire by hydrochloric acid and sulfuric acid. *Advanced Materials Research*, *626*, 706–710. https://doi.org/10.4028/www.scientific.net/AMR.626.706

Smith, B. C. (2024). *FTIR Spectrometer: Konsep, Prinsip Kerja, dan Aplikasinya*. https://warstek.com/spectrometer-ftir/

Tan, I. A. W., Abdullah, M. O., Lim, L. L. P., & Yeo, T. H. C. (2017). Surface modification and characterization of coconut shell-based activated carbon subjected to acidic and alkaline treatments. *Journal of Applied Science & Process Engineering*, *4*(2), 186–194. https://doi.org/10.33736/jaspe.435.2017

Tani, D., & Lumingkewas, S. (2022). Pembuatan dan karakterisasi karbon aktif dari arang tempurung kelapa dengan kombinasi aktivasi kimia dan fisika. *Fullerene Journal of Chemistry*, *7*(2), 124–132.

Timur, S., Kantarli, I. C., Ikizoglu, E., & Yanik, J. (2006). Preparation of activated carbons from *Oreganum* stalks by chemical activation. *Energy & Fuels*, *20*(6), 2636–2641. https://doi.org/10.1021/ef060219k

Tosin, O. V., Gabriel, S. S., Wukatda, S. S., Simon I, I., Mhd, I., & Bolong, A.-M. A. (2021). Fillet y ield and length-weight relationship of five fish species from lower River Benue, Makurdi, Nigeria. *Tropical Life Sciences Research*, *32*(1), 163–174. https://doi.org/10.21315/tlsr2021.32.1.10

Vasdazara, O. L., Ardhyananta, H., & Wicaksono, S. T. (2018). Pengaruh penambahan serat cangkang kelapa sawit (palm kernel fiber) terhadap sifat mekanik dan stabilitas termal komposit epoksi/serat cangkang kelapa sawit. *Jurnal Teknik ITS*, *7*(1), F119–F123. https://doi.org/10.12962/j23373539.v7i1.28200

Verayana, V., Paputungan, M., & Iyabu, H. (2018). Pengaruh aktivator HCl dan H_3PO_4 terhadap karakteristik (morfologi pori) arang aktif tempurung kelapa serta uji adsorpsi pada logam timbal (Pb). *Jurnal Entropi*, *13*(1), 67–75.

Wulandari, R., Riyanto, C. A., & Martono, Y. (2023). Kinerja karbon aktif daun eceng gondok pada penurunan kadar fosfat artifisial dan surfaktan dalam limbah detergen. *ALCHEMY Jurnal Penelitian Kimia*, *19*(2), 149–161. https://doi.org/10.20961/alchemy.19.2.65626.149-161

Yakout, S. M., & El-Deen, G. S. (2016). Characterization of activated carbon prepared by phosphoric acid activation of olive stones. *Arabian Journal of Chemistry*, *9*, S1155–S1162. https://doi.org/10.1016/j.arabjc.2011.12.002